Liu et al. European Radiology Experimental (2025)9:50
https://doi.org/10.1186/s41747-025-00590-1

EUROPEAN SOCIETY OF RADIOLOGY
European Radiology
EXPERIMENTAL

ORIGINAL ARTICLE Open Access

Comparison of four MRI diffusion models to differentiate benign from metastatic retropharyngeal lymph nodes

Jun Liu[1,2], Li Hua[3], Fei Wang[2], Ming Chen[2], Yinan Sun[2], Zhi Hu[2], Luqing Shu[2], Andong He[2], Mengxiao Liu[4], Qing Yang[2,5*], Juan Zhu[2*] and Yinfeng Qian[1*]

Abstract

Background Conventional magnetic resonance diffusion-weighted imaging (DWI) and morphological features have limitations in distinguishing benign from metastatic retropharyngeal lymph nodes (RLNs). We aimed to compare the value of continuous-time random walk (CTRW), fractional-order calculus (FROC), stretched-exponential model (SEM), and conventional DWI, in combination with morphological features, for differentiating between the two groups.

Methods Fifty-nine patients with 68 RLNs (23 benign and 45 metastatic) were enrolled. All patients underwent DWI with 12 *b*-values. Diffusion data were reconstructed using conventional DWI, SEM, FROC, and CTRW models, yielding nine parameters: apparent diffusion coefficient (ADC), distributed diffusion coefficient $(DDC)_{SEM}$, α_{SEM}, D_{FROC}, β_{FROC}, μ_{FROC}, D_{CTRW}, α_{CTRW}, and β_{CTRW}. Diffusion parameters and morphological features were compared using Mann–Whitney *U*, independent sample *t*, or χ^2 tests. Logistic regression analysis was performed to identify the best diffusion indicator for classification and to develop a multiparameter model combining morphological features. Area under the receiver operating curve (AUC) and DeLong tests were used.

Results Significant differences in diffusion parameters were found between benign and metastatic RLNs, except for α_{CTRW} ($p \le 0.022$). Benign RLNs exhibited higher ADC, DDC_{SEM}, D_{FROC}, and D_{CTRW}, while metastatic RLNs had higher α_{SEM}, β_{FROC}, μ_{FROC}, and β_{CTRW}. Multivariate logistic regression analysis identified β_{CTRW} as the optimal single diffusion indicator (AUC = 0.913). The combined model of β_{CTRW} with morphological features further improved diagnostic performance and yielded an AUC of 0.948.

Conclusion β_{CTRW} is an effective noninvasive biomarker for distinguishing between benign and metastatic RLNs. Thus, combining β_{CTRW} with morphological features enhances diagnostic efficiency.

Relevance statement This study demonstrates that β_{CTRW}, derived from the continuous-time random walk diffusion model, when integrated with morphological features, offers a reliable, noninvasive diagnostic approach for differentiating between benign and metastatic retropharyngeal lymph nodes.

*Correspondence:
Qing Yang
56469225@qq.com
Juan Zhu
55522670@qq.com
Yinfeng Qian
894206876@qq.com
Full list of author information is available at the end of the article

Key Points

- Non-Gaussian diffusion metrics outperformed conventional DWI.
- β_{CTRW} was the best indicator for distinguishing benign from metastatic lymph nodes.
- Combining β_{CTRW} with minimal axial diameter further improved diagnostic efficiency.

Keywords Diffusion magnetic resonance imaging, Lymph nodes, Magnetic resonance imaging, Neoplasm metastasis, Retropharyngeal space

Graphical Abstract

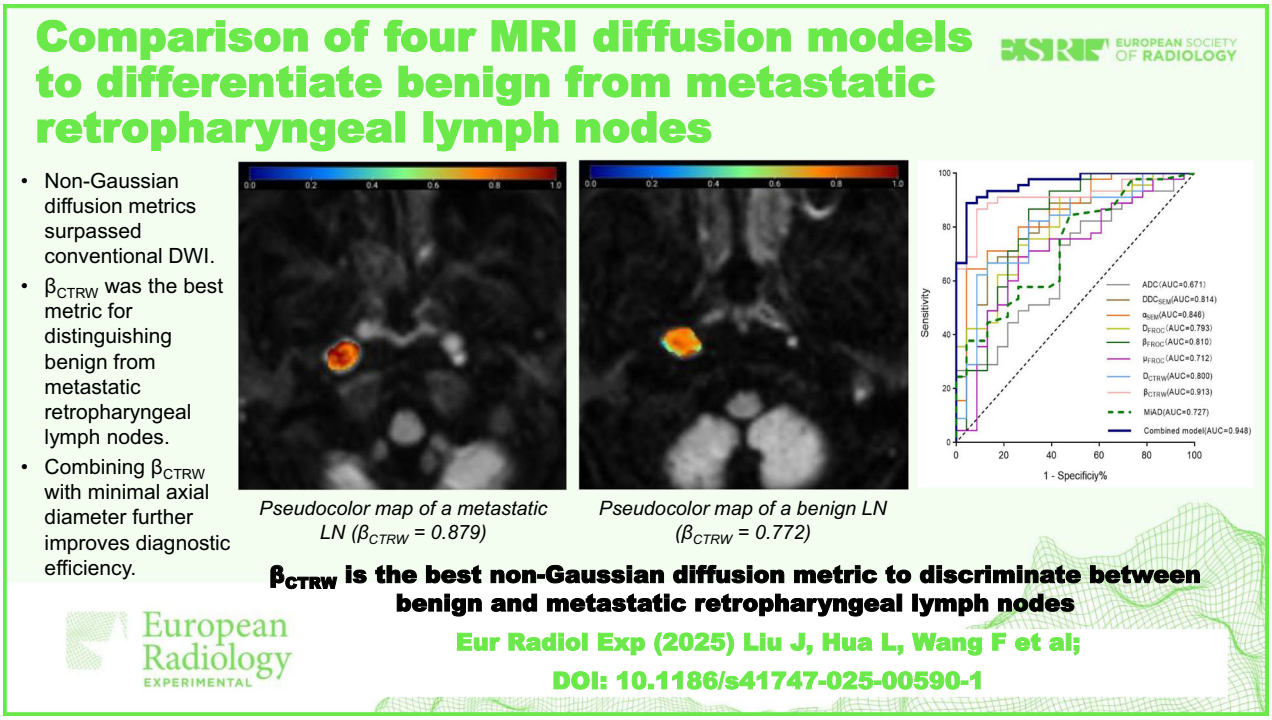

Background

Nasopharyngeal carcinoma (NPC) is a head and neck cancer associated with the Epstein–Barr virus (EBV), with a high prevalence in southern China and Southeast Asia [1]. It is the most common malignancy leading to metastasis in the retropharyngeal lymph nodes (RLNs), with lymph node metastasis rate exceeding 60% [2–4]. RLNs serve as the first echelon of lymph nodes for NPC metastasis and are independent prognostic indicators [5, 6]. In patients with NPC, cervical lymph nodes < 1.0 cm in diameter are frequently observed, and distinguishing between inflammatory and metastatic lymph nodes is challenging due to overlapping features [7, 8]. Metastatic spread in NPC follows a predictable pattern, with RLN involvement correlating with cervical lymph node metastasis in all neck regions except zone I [2, 8]. Therefore, an accurate assessment of RLN status is critical for evaluating suspected metastatic small lymph nodes in other cervical regions [7–9]. The presence of metastatic RLNs significantly influences treatment choices for patients with NPC, particularly those with stage T1–T3 disease [10]. Specifically, RLN involvement affects the delineation of the clinical target volume of the primary tumor as well as the dosage and extent of radiotherapy [7, 11]. Consequently, precise assessment of RLN metastasis is essential for staging, treatment planning, and prognosis determination.

However, evaluating RLNs is challenging due to their deep anatomical location. The difficulty of surgical clearance and the limited feasibility of biopsy in NPC, which is primarily not surgically treated. Therefore, imaging, particularly magnetic resonance imaging (MRI), plays a crucial role in RLN assessment [1, 11, 12]. RLN metastasis is typically evaluated through clinical and imaging follow-up, with a minimum axial diameter (MiAD) threshold of 5 or 6 mm serving as a diagnostic criterion [13, 14]. However, patients with nasopharyngeal

lymphoid hyperplasia and EBV often develop reactive RLN enlargement [15]. This presents a significant overlap between benign reactive hyperplastic and metastatic lymph nodes [16, 17]. Therefore, reliance on MiAD as a diagnostic criterion may result in the misdiagnosis of benign reactive hyperplastic lymph nodes as metastatic.

Diffusion MRI is a widely used noninvasive technique for assessing tissue microcirculation and has demonstrated utility in lymph node evaluation [16, 17], offering insights beyond the conventional morphological characterization of lesions [16–21]. Previous studies have reported low apparent diffusion coefficient (ADC) values in metastatic RLNs [18–20]. However, So et al [21] reported contradictory findings. Furthermore, the existing literature indicates suboptimal diagnostic performance of ADC parameters in differentiating benign from metastatic RLNs, with reported area under the receiver operating characteristic curve (AUC) values consistently below 0.75 [18, 19]. Conventional diffusion-weighted imaging (DWI) models assume a Gaussian distribution of water molecule diffusion, failing to account for tissue heterogeneity [22–38], thereby greatly limiting their applicability [22]. To overcome this limitation, alternative diffusion models, including stretched-exponential (SEM) [22–24], fractional-order calculus (FROC) [25–32], and continuous-time random walk (CTRW) diffusion models [30–38] have been introduced to better characterize non-Gaussian diffusion distribution of water molecule in highly heterogeneous tumor.

The SEM model quantifies intravoxel heterogeneity using the distributed diffusion coefficient (DDC_{SEM}) and diffusion heterogeneity coefficient (α_{SEM}) [22–24]. SEM can reflect pathological characteristics, the heterogeneity of intravoxel diffusion rates, and the distribution of diffusion effects within multiple water molecule pools in each voxel. Several studies [22–24] have demonstrated that SEM can characterize lesions, such as breast cancer or solid hepatic masses. The FROC model characterizes tissue heterogeneity through three parameters: the derived diffusion coefficient (D_{FROC}), spatial fractional-order parameter (β_{FROC}), and spatial parameter (μ_{FROC}) [25–29]. The FROC model has shown potential in lesion classification, tumor grading, and typing [25–32]. The CTRW model reflects the intratumoral cell density and microstructural heterogeneity through three quantitative parameters: the diffusion constant (D_{CTRW}), temporal diffusion parameter (α_{CTRW}), and spatial diffusion parameter (β_{CTRW}) [33–38]. The CTRW model has been validated in characterizing lesions in the central nervous system, breast, and prostate [31–38]. However, it remains unclear whether the diffusion parameters derived from the CTRW, FROC, and SEM models can effectively differentiate benign from metastatic RLNs. Furthermore, it is uncertain whether these diffusion models outperform ADC values and traditional morphological features in RLN differentiation.

This study aims to determine the value of diffusion parameters derived from conventional DWI, SEM, FROC, and CTRW models, either individually or in combination, in differentiating benign RLNs in plasma EBV-positive patients from metastatic RLNs in NPC patients. Furthermore, we seek to identify morphological differences between the two groups of lymph nodes. Additionally, we sought to evaluate the diagnostic efficacy of these diffusion parameters when combined with morphological features, thus improving valuable references for optimizing N staging and outlining radiotherapy targets.

Methods

Patient population

This retrospective study, approved by the Medical Ethics Committee of our hospital, included patients who underwent DWI with 12 *b*-values for the nasopharyngeal region between January 2022 and August 2023. Of 80 patients initially considered, 21 were excluded due to the absence of assessable RLNs or lymph nodes with a MiAD < 6.0 mm ($n = 14$), severe DWI artifacts ($n = 4$), or prior chemotherapy or radiotherapy ($n = 3$). The final cohort comprised 59 patients with 68 RLNs (23 benign and 45 metastatic).

The inclusion criteria for benign RLNs were as follows: (1) EBV deoxyribonucleic acid—DNA positivity with MRI evaluation for nasopharyngeal soft tissue thickening and a final pathological diagnosis of lymphoid hyperplasia; (2) absence of NPC or other head and neck tumors confirmed by MRI and endoscopy, with at least 1-year follow-up; (3) MiAD ≥ 6.0 mm; (4) no previous history of autoimmune diseases or malignancies.

Metastatic RLNs were defined as follows: (1) pathologically confirmed NPC with RLN coverage on nasopharyngeal DWI; (2) presence of at least one lymph node with a MiAD ≥ 6.0 mm, necrosis, or extranodal extension; (3) lymph node resolution after at least 1-year follow-up after NPC treatment.

The inclusion criteria for benign and metastatic RLNs were based on guidelines from previous studies [20, 21]. The RLNs selection process is shown in Fig. 1.

MRI acquisition

MRI scans were performed using a 3.0-T whole-body system (MAGNETOM Vida, Siemens Healthcare, Erlangen, Germany) with a 20-channel head and neck phased array coil. The scanning sequence protocol included the following:

1. Coronal T2-weighted imaging with fat saturation: repetition time (TR) = 4,330 ms; echo time = 86 ms;

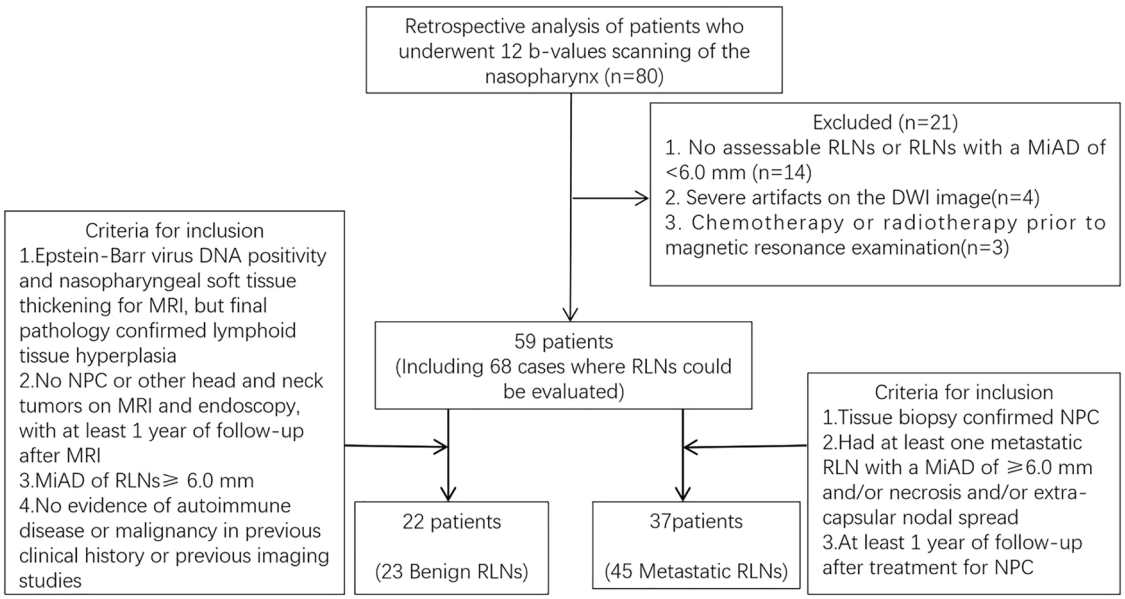

Fig. 1 Flow chart of RLNs selection in this study. MiAD, Minimal axial diameter; NPC, Nasopharyngeal carcinoma; RLNs, Retropharyngeal lymph nodes

field of view = 25 × 25 cm; slice thickness = 4 mm; slice gap = 1 mm; number of excitations = 1;

2. Axial T1-weighted imaging: repetition time = 463 ms; echo time = 6.5 ms; field of view = 20 × 20 cm; slice thickness = 4 mm; slice gap = 1 mm; number of excitations = 3;
3. Axial T2-weighted imaging with fat saturation: TR = 4,330 ms; TE = 86 ms; FOV = 20 × 20 cm; slice thickness = 4 mm; slice gap = 1 mm; number of excitations = 2;
4. DWI sequence using "Readout Segmentation of Long Variable Echo-trains"—RESOLVE, with 12 *b*-values (0, 10, 20, 50, 100, 200, 400, 800, 1,000, 1,500, 2,000, and 3,000 s/mm^2), with a single excitation for each *b*-value. The specific parameters were field of view = 22 × 22 cm; repetition time = 3,800 ms; echo time = 70 ms; slice thickness = 4 mm; slice gap factor = 20%; readout segments = 5; number of slices = 22; simultaneous multi-slice = 2; diffusion mode = 3-scan trace; scanning time is approximately 7 min;
5. Finally, contrast-enhanced T1-weighted imaging scans were performed in axial, coronal, and sagittal planes with an intravenous injection of gadodiamide (Omniscan, GE Healthcare Ireland Ltd, Cork, Ireland) at a flow rate of 2.5 mL/s (total dose of 0.1 mmol/kg) via the median cubital vein.

Image analysis

Diffusion parameters from conventional DWI, SEM, FROC, and CTRW were processed using Body DiffusionLab (BoDiLab, Chengdu ZhongYing Medical Technology Co., Ltd, Chengdu, China) software on a workstation. The final pseudocolor map was generated with ITK-SNAP software http://www.itksnap.org/pmwiki/pmwiki.php.

For conventional DWI, ADC was generated by fitting a single-exponential model using Eq. 1:

$$\frac{S(b)}{S(0)} = \exp(-b \cdot ADC) \tag{1}$$

where S(b) represents signal intensity and $S(0)$ is the signal intensity without diffusion weighting. The diffusion weighting factor b determines the degree of diffusion weighting in the signal intensity.

The SEM model is fitted using Eq. 2:

$$\frac{S(b)}{S(0)} = \exp[-(b \cdot DDC)^{\alpha}] \tag{2}$$

The distributed diffusion coefficient (DDC) is the diffusion coefficient of the stretched-exponential model, α is the heterogeneity index (dimensionless), and b is a complex factor related to diffusion gradient strength and diffusion time.

The FROC model is represented by Eq. 3:

$$\frac{S(b)}{S(0)} = \exp\left[-D\mu^{2(\beta-1)}(\gamma G_{d\delta})^{2\beta}\left(\Delta - \frac{2\beta-1}{2\beta+1}\delta\right)\right] \tag{3}$$

where G_d is the diffusion gradient amplitude, Δ is the gradient interval, and δ is the diffusion gradient pulse width. The parameter β is the intravoxel diffusion heterogeneity parameter, and μ is the spatial diffusion parameter used to retain the nominal units of D in mm^2/s. The diffusion images were fitted to the FROC model using

the Levenberg–Marquardt nonlinear fitting algorithm [39]. During the fitting process, lower *b*-values (≤ 1,000 s/mm²) were used to estimate *D* with a monoexponential model. β and μ were derived from image fitting using all *b*-values after *D* was determined.

The CTRW model is fitted using Eq. 4:

$$\frac{S(b)}{S(0)} = E_{\alpha}[(-bD)^{\beta}] \quad (4)$$

where *D* is the anomalous diffusion coefficient, estimated by nonlinear fitting of diffusion images with *b*-values ≤ 1,000 s/mm². α and β are parameters related to temporal and spatial diffusion heterogeneity, respectively, and are determined simultaneously from all diffusion-weighted images.

All lymph node size, signal homogeneity, lymph node borders and diffusion parameters were independently assessed in a blinded manner by two observers with 10 (J.L.) and 15 years (F.W.) of experience in diagnosing head and neck tumors. Using T1-weighted images as references, the maximum and minimal axial diameter of lymph nodes were measured on T2-weighted with fat saturation imaging and further categorized into three dimensions (≥ 6 mm, < 8 mm, ≥ 8 mm, < 10 mm, and ≥ 10 mm) according to the classification methodology established in a previous study [17]. MiAD was defined as the maximum value in the axial plane of the lymph node perpendicular to the maximum axial diameter. Signal homogeneity is categorized into homogeneous and heterogeneous changes. Lymph node borders were categorized as clear or unclear based on the presence or absence of extraperitoneal spread.

The multi-*b*-value diffusion images were initially imported into the Body DiffusionLab post-processing software, where image registration was performed to ensure accurate alignment. Subsequently, the software applied the mathematical formulas of the CTRW, FROC, SEM, and conventional DWI models to perform pixel-wise fitting. By comparing the signal intensity at each pixel with different *b*-values, the software calculated multiple diffusion-related parameters, which were then presented as pseudocolor maps. Region of interest (ROI) was manually delineated on DWI with a *b*-value of 1,000 s/mm², ensuring the exclusion of necrotic areas, cystic changes, and adjacent anatomical structures. The software then automatically propagated the delineated ROIs across all nine diffusion parameter maps and computed the corresponding values (Figs. 2 and 3). Another independent observer with 20 years of experience in MRI (J.Z.) reviewed the ROIs delineated by the two radiologists and resolved any disputes regarding lymph node borders and signal homogeneity.

The mean values of the two observers' measurements were used as final parameter values, and the interclass correlation coefficients were calculated to assess interobserver agreement. The same observers repeated the measurements after a 1-month interval, and intragroup correlation coefficients were computed to evaluate intraobserver reliability.

Statistical analysis

Quantitative parameters were tested for normality. Normally distributed data were represented as mean ± standard deviation ($\overline{X} \pm S$), whereas those with a skewed distribution were represented as median *(P25, P75)*. Data analyses were performed using MedCalc v.22.01 (MedCalc Software Ltd, Ostend, Belgium), SPSS v.23.0 (IBM Corp, Armonk, NY, USA), and GraphPad Prism v.8.0 (GraphPad Software, San Diego, CA, USA). Differences between noncategorical data were assessed using independent sample *t* or Mann–Whitney *U* tests. Categorical data were compared using χ^2 tests. Significant parameters ($p < 0.050$) identified via binary logistic regression analysis were used to construct a multiparametric diagnostic model and generate the corresponding odds ratios. Receiver operating characteristic curves were generated to assess diagnostic performance, with area under the curves (AUCs) compared using the DeLong test. Interobserver consistency was evaluated using intraclass correlation coefficients with 95% confidence intervals. A two-sided test with $p < 0.050$ was considered statistically significant.

Results

Clinical characteristics and grouping of participants

The study analyzed 23 benign and 45 metastatic RLNs from 59 patients. No significant differences were observed in maximum axial diameter, T2 signal homogeneity, sex, age, or borders between benign and metastatic RLNs. However, the MiAD of metastatic RLNs was significantly larger than that of benign RLNs (Table 1).

Repeatability of diffusion parameters and lymph node size

The intraclass correlation coefficient values for the DWI parameters ranged between 0.835 and 0.959, those for lymph node size ranged between 0.918 and 0.985, indicating good intra- and interobserver agreement for all quantitative parameters (Table 2).

Differences in each diffusion parameter between benign and metastatic RLNs

Except for α_{CTRW}, all eight diffusion parameters differed significantly between benign and metastatic RLNs. Benign RLNs exhibited higher ADC, DDC_{SEM}, D_{FROC}, and D_{CTRW} values, whereas metastatic RLNs had higher α_{SEM}, β_{FROC}, μ_{FROC}, and β_{CTRW} values (Fig. 4; Table 3).

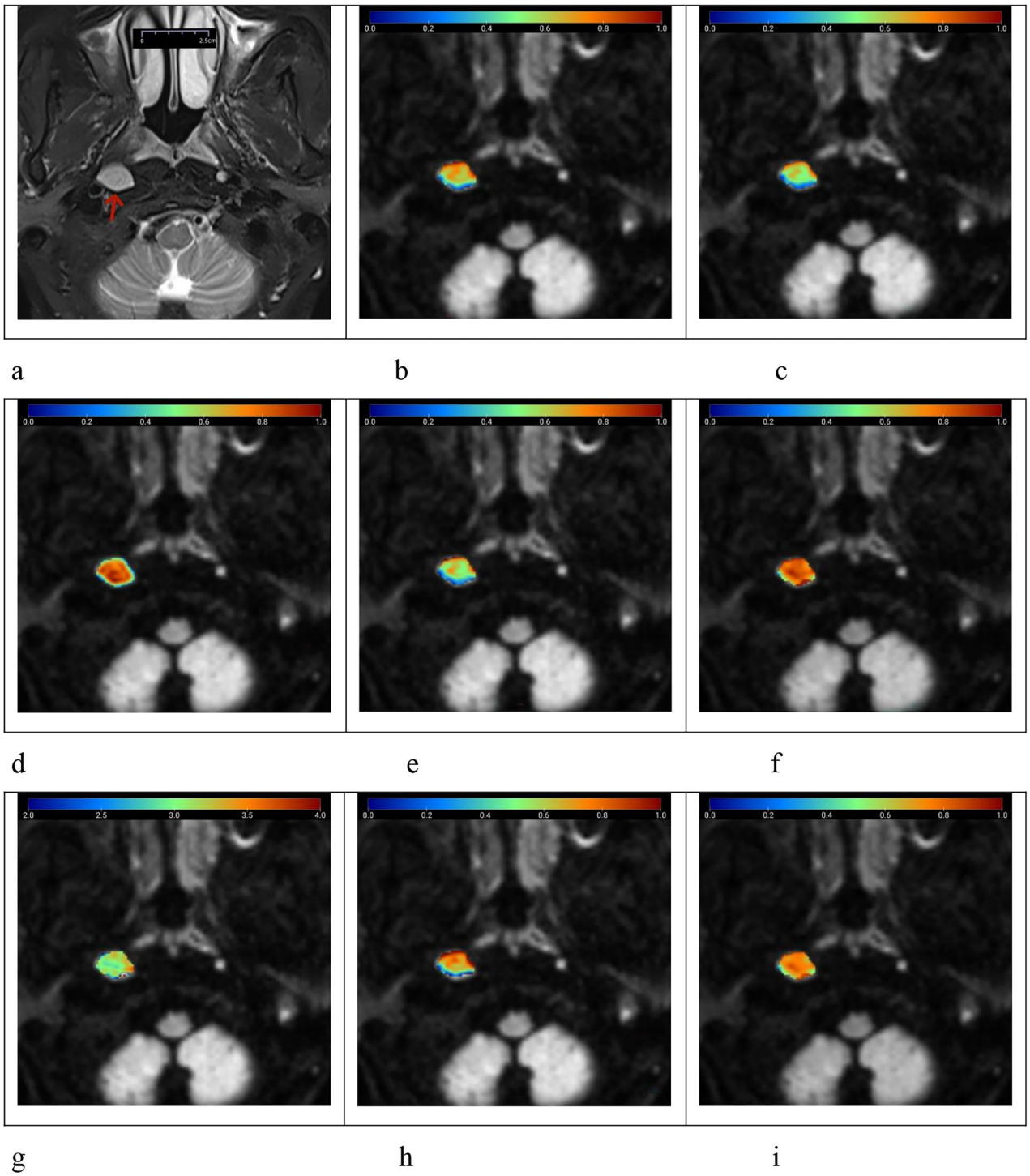

Fig. 2 Female patient, aged 45 years, with nasopharyngeal lymphoid hyperplasia and Epstein–Barr virus positivity, presenting with a benign right retropharyngeal lymph node (arrow). **a** T2-weighted imaging with fat saturation shows the lymph node with a maximum axial diameter of 1.58 cm and minimal axial diameter of 1.14 cm, exhibiting a homogeneously slightly high signal. **b**–**i** Pseudocolor maps of the quantitative parameters ADC = 0.678 μm^2/ms (**b**), DDC_{SEM} = 0.616 μm^2/ms (**c**), α_{SEM} = 0.740 (**d**), D_{FROC} = 0.597 μm^2/ms (**e**), β_{FROC} = 0.815 (**f**), μ_{FROC} = 3.289 μm (**g**), D_{CTRW} = 0.721 μm^2/ms (**h**), and β_{CTRW} = 0.772 (**i**), derived from conventional DWI, SEM, FROC, and CTRW diffusion models. ADC, Apparent diffusion coefficient; CTRW, Continuous-time random walk; DDC, Distributed diffusion coefficient; DWI, Diffusion-weighted imaging; FROC, Fractional-order calculus; SEM, Stretched-exponential model

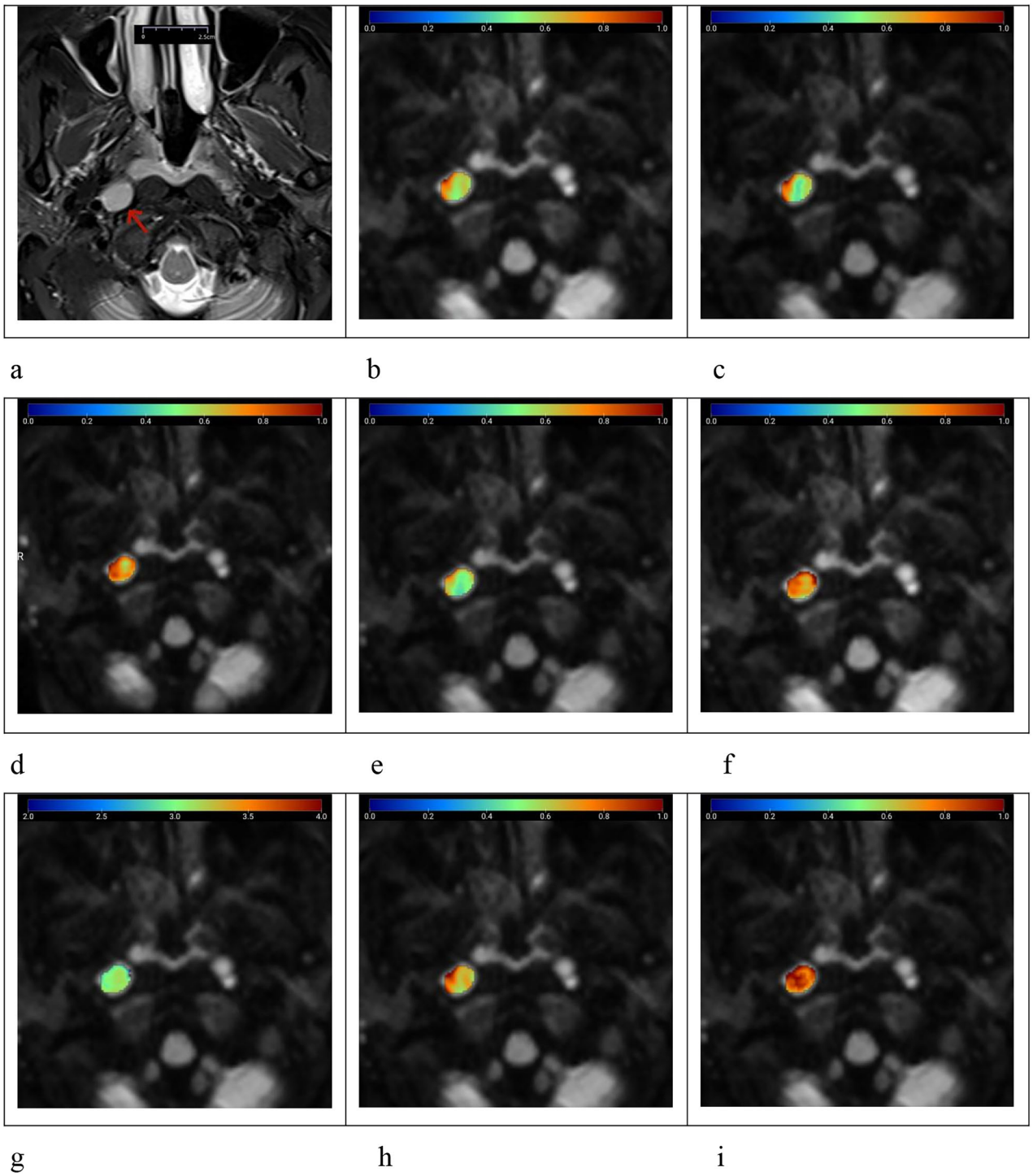

Fig. 3 Female patient, aged 51 years, with nasopharyngeal non-keratinizing squamous carcinoma and a metastatic right retropharyngeal lymph node (arrow). **a** T2-weighted imaging with fat saturation shows the lymph node with a homogeneously slightly high signal, a maximum axial diameter of 1.19 cm, and minimal axial diameter of 0.93 cm. **b**–**i** Pseudocolor maps of the quantitative parameters ADC = 0.630 μm^2/ms (**b**), DDC_{SEM} = 0.612 μm^2/ms (**c**), α_{SEM} = 0.755 (**d**), D_{FROC} = 0.589 μm^2/ms (**e**), β_{FROC} = 0.829 (**f**), μ_{FROC} = 3.107 μm (**g**), D_{CTRW} = 0.740 μm^2/ms (**h**), and β_{CTRW} = 0.879 (**i**), derived from conventional DWI, SEM, FROC, and CTRW diffusion models. ADC, Apparent diffusion coefficient; CTRW, Continuous-time random walk; DDC, Distributed diffusion coefficient; DWI, Diffusion-weighted imaging; FROC, Fractional-order calculus; SEM, Stretched-exponential model

Diagnostic performances of diffusion parameters and MiAD in benign and metastatic RLNs

Univariate binary logistic regression analysis identified DDC_{SEM}, α_{SEM}, D_{FROC}, β_{FROC}, μ_{FROC}, D_{CTRW}, and β_{CTRW} as significant predictors for distinguishing benign from metastatic RLNs. Receiver operating characteristic curve analysis showed that β_{CTRW} exhibited the highest diagnostic efficacy, with an AUC of 0.913, cutoff value of 0.830, sensitivity of 86.7%, and specificity of 91.3%. In contrast, ADC demonstrated the lowest diagnostic efficacy (AUC = 0.671, cutoff value = 0.686 $\mu m^2/ms$, sensitivity = 82.2%, specificity of 47.8%). The MiAD yielded an AUC of 0.727, cutoff value of 9.3 mm, with 84.4% sensitivity and 52.2% specificity. The DeLong test revealed significant differences between β_{CTRW} and ADC, μ_{FROC}, and MiAD ($p = 0.002$, 0.008, 0.013), as well as between DDC_{SEM}, D_{FROC}, D_{CTRW}, and ADC ($p = 0.002$, 0.002, 0.014).

Multivariate logistic regression analysis identified β_{CTRW} as the most effective single integrated indicator. Combining β_{CTRW} with MiAD further improved diagnostic performance (AUC = 0.948, sensitivity = 91.1%, specificity = 87.0%). This combination model showed significant AUC differences compared with DDC_{SEM}, α_{SEM}, D_{FROC}, β_{FROC}, μ_{FROC}, D_{CTRW}, ADC, and MiAD ($p = 0.021$, 0.044, 0.011, 0.013, 0.001, 0.022, < 0.001, < 0.001), but not with β_{CTRW} alone ($p = 0.165$; Tables 4 and 5; Fig. 5).

Table 1 Patient characteristics of benign and metastatic RLNs

Characteristic	Benign RLNs	Metastatic RLNs	*p*-value
Sex			0.122
Male	12	31	
Female	11	14	
Age (years)	53.5 ± 10.6	56.4 ± 13.2	0.341
Maximum axial diameter			
≥ 6 mm, < 10 mm	6	20	0.913
≥ 10 mm, < 20 mm	17	24	
≥ 20 mm	0	1	
Minimal axial diameter			0.005
≥ 6 mm, < 8 mm	13	21	
≥ 8 mm, < 10 mm	9	8	
≥ 10 mm	1	16	
Signal homogeneity			0.673
Homogeneous	16	29	
Heterogeneous	7	16	
Border			0.551
Well defined	20	35	
Ill-defined	3	9	

RLNs Retropharyngeal lymph nodes

Discussion

This study evaluated the clinical value of four diffusion model parameters and lymph node morphological characteristics in distinguishing between benign and metastatic RLNs. The results indicate that some non-Gaussian diffusion parameters, particularly β_{CTRW}, outperform conventional ADC and MiAD in differentiating benign from metastatic RLNs. Moreover, the combined model of β_{CTRW} and MiAD demonstrates a higher AUC, contributing to improved diagnostic efficiency.

This study found that metastatic RLNs exhibited lower ADC values than benign hyperplastic lymph nodes, suggesting increased cell density in metastatic lymph nodes. This finding aligns with the results of Wang et al [18–20]. However, So et al [21] reported lower ADC values in benign RLNs, possibly due to variations in ROI delineation, *b*-value selection, and scanning protocols [40–42]. Furthermore, single-shot echo-planar imaging can

Table 2 Reproducibility of DWI parameters and lymph node size

Parameters	Intraobserver (95% CI)	Interobserver (95% CI)
ADC ($\times 10^{-3}$ mm^2/s)	0.896 (0.831–0.936)	0.908 (0.851–0.943)
DDC_{SEM} ($\times 10^{-3}$ mm^2/s)	0.935 (0.894–0.960)	0.940 (0.903–0.963)
α_{SEM}	0.859 (0.771–0.913)	0.898 (0.834–0.937)
D_{FROC} ($\times 10^{-3}$ mm^2/s)	0.944 (0.910–0.966)	0.941 (0.905–0.964)
β_{FROC}	0.884 (0.811–0.928)	0.909 (0.852–0.944)
μ_{FROC} (μm)	0.923 (0.875–0.953)	0.909 (0.853–0.944)
D_{CTRW} ($\times 10^{-3}$ mm^2/s)	0.953 (0.924–0.971)	0.949 (0.917–0.968)
α_{CTRW}	0.947 (0.914–0.967)	0.952 (0.922–0.970)
β_{CTRW}	0.959 (0.934–0.975)	0.950 (0.918–0.969)
Maximum axial diameter	0.918 (0.871–0.949)	0.969 (0.950–0.981)
MiAD	0.985 (0.976–0.991)	0.973 (0.957–0.983)

ADC Apparent diffusion coefficient, *CI* Confidence interval, *CTRW* Continuous-time random walk, *DWI* Diffusion-weighted imaging, *FROC* Fractional-order calculus, *MiAD* Minimal axial diameter, *SEM* Stretched-exponential model

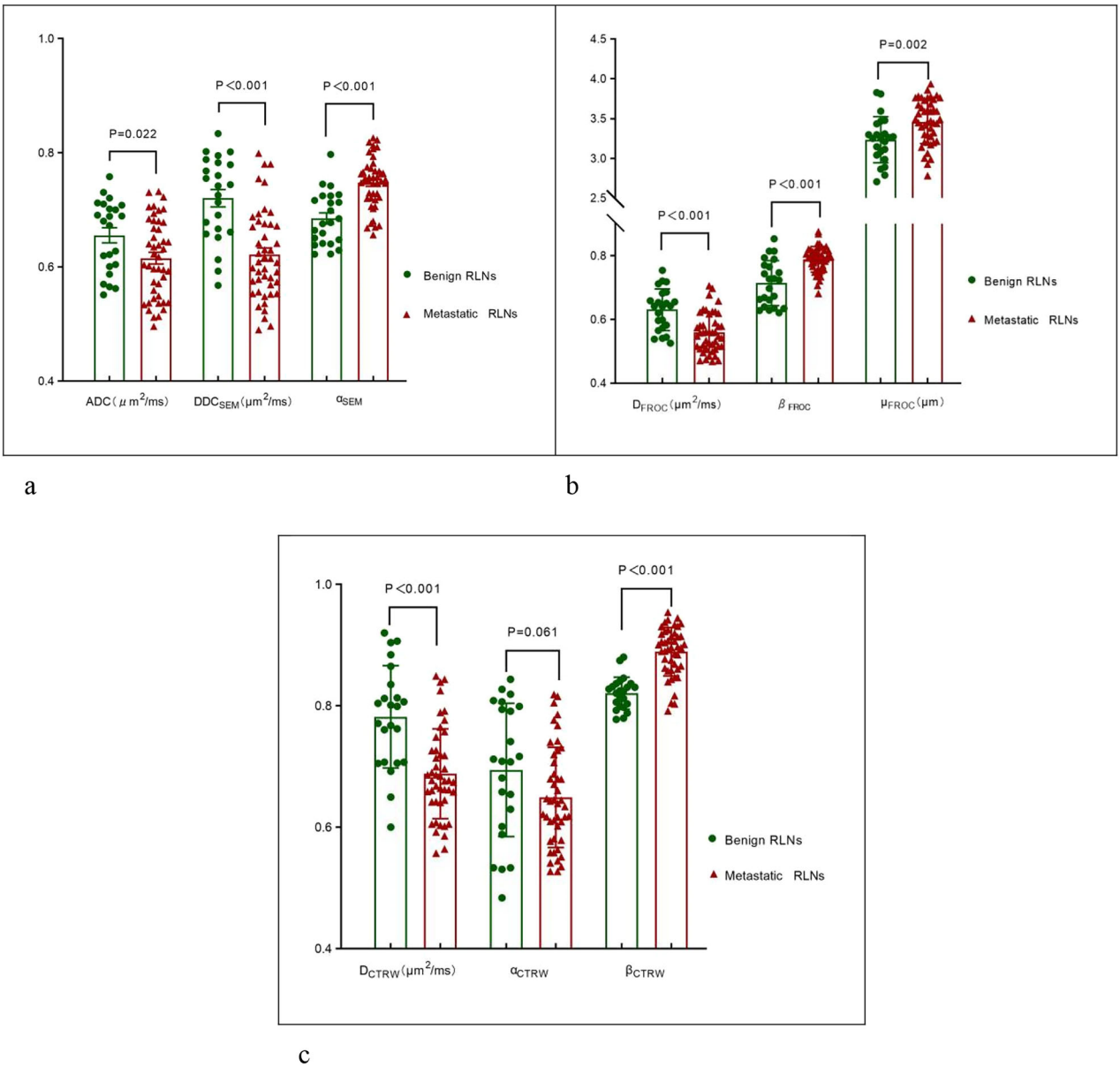

Fig. 4 Box plots and scatter plots showing differences in quantitative diffusion parameters between benign and metastatic retropharyngeal lymph nodes. ADC, Apparent diffusion coefficient; CTRW, Continuous-time random walk; FROC, Fractional-order calculus; SEM, Stretched-exponential model. **a** Differences between parameters obtained from conventional DWI and the stretched-exponential model (SEM). **b** Differences between parameters obtained from the fractional-order calculus (FROC) model. **c** Differences between parameters obtained from the continuous-time random walk (CTRW) model.

introduce geometric distortions and artifacts, potentially affecting data stability.

Unlike previous studies on RLNs [17–21], this study simultaneously incorporated three non-Gaussian models (CTRW, FROC, and SEM) to capture differences between benign and metastatic RLNs using multiple diffusion parameters that reflect tissue heterogeneity. Furthermore, we compared the diagnostic efficacy of these models against ADC values and incorporated morphological features for a comprehensive analysis. To enhance data stability, we utilized the "Readout Segmentation of Long Variable Echo-trains"—RESOLVE sequence for image acquisition, thereby reducing distortions and artifacts in DWI images [43]. Previous studies have confirmed the utility of these models in lesion staging, identification, and efficacy assessment [22–38]; however, their application to RLNs remains unexplored.

DDC_{SEM} reflects the average diffusion rate within a voxel and represents a weighted sum of ADC values from multiple exponential decay components, exhibiting a strong positive correlation with ADC [23]. In this study, the correlation coefficient between DDC_{SEM} and ADC was 0.797 ($p < 0.001$), which is consistent with previous findings. D_{FROC}, derived from fitting multiple *b*-values below 1,000 s/mm², functions similarly to diffusion coefficients in other diffusion models. It reflects tumor cell density, cell membrane integrity, and other structural properties influencing water diffusion in tissues, making it a more physiologically relevant indicator of true tissue diffusion [25–30]. D_{CTRW}, similar to ADC, measures tissue cell density [31, 32]. However, unlike ADC, D_{CTRW} accounts for non-Gaussian diffusion behavior [33–38].

Table 3 Comparisons of DWI parameters between benign and metastatic RLNs

Parameters	Benign RLNs	Metastatic RLNs	Z/T value	*p*-value
ADC (μm²/ms)	0.655 ± 0.063	0.615 ± 0.068	2.343	0.022[a]
DDC_{SEM} (μm²/ms)	0.721 ± 0.073	0.622 ± 0.077	5.077	< 0.001[a]
α_{SEM}	0.685 ± 0.047	0.748 ± 0.044	-5.456	< 0.001[a]
D_{FROC} (μm²/ms)	0.631 ± 0.065	0.559 ± 0.061	4.473	< 0.001[a]
β_{FROC}	0.714 ± 0.071	0.789 ± 0.040	-4.155	< 0.001[b]
μ_{FROC} (μm)	3.235 ± 0.291	3.461 ± 0.278	-3.148	0.002[a]
D_{CTRW} (μm²/ms)	0.782 ± 0.084	0.688 ± 0.074	4.709	< 0.001[a]
α_{CTRW}	0.694 ± 0.110	0.649 ± 0.082	1.908	0.061[a]
β_{CTRW}	0.821 ± 0.027	0.889 ± 0.040	-5.542	< 0.001[b]

ADC Apparent diffusion coefficient, *CTRW* Continuous-time random walk model, *DWI* Diffusion-weighted imaging, *FROC* Fractional-order calculus model, *RLNs* Retropharyngeal lymph nodes, *SEM* Stretched-exponential model
[a] Independent sample *t*-tests
[b] Mann–Whitney U test

Compared with benign RLNs, metastatic RLNs exhibit increased cell density and abnormal proliferation, leading to more pronounced restricted water diffusion and lower values for these parameters. These findings are consistent with previous studies of prostate, breast and clear cell carcinoma of the kidney [27–29, 32, 33, 38].

μ_{FROC} is a measure of the average free diffusion length and is inversely correlated with tissue cellularity [28, 29]. In malignant tumors, abnormal cell proliferation restricts water molecule diffusion, leading to higher μ_{FROC} values. Previous studies have demonstrated that malignant breast lesions and high-grade bladder tumors exhibit higher μ_{FROC} values. In this study, the μ_{FROC} value of metastatic lymph nodes was lower, aligning with these earlier findings [28, 29].

α_{SEM} measures the deviation of signal decay characteristics within a voxel from the single-exponential model, with lower α_{SEM} values indicating greater inhomogeneity in exponential decay [22, 23]. In this study, benign RLNs exhibited relatively low α_{SEM} values, similar to the findings of Seo [24], who reported lower α_{SEM} values in hepatic hemangiomas compared to hepatic metastases. β_{FROC} quantifies tissue homogeneity, reflecting increased heterogeneity within a voxel [25–30]. Previous studies have demonstrated that malignant lesions typically exhibit lower β_{FROC} values [28, 29]. In this study, benign lymph nodes undergoing reactive hyperplasia showed increased proliferation of cells, such as lymphocytes, macrophages, and plasma cells, in response to viral or other stimuli [44, 45]. This resulted in increased inhomogeneity and heterogeneity in exponential decay within voxels, leading to lower α_{SEM} and β_{FROC} values.

The parameters α_{CTRW} and β_{CTRW} are novel indicators reflecting temporal and spatial diffusion heterogeneity, respectively. In a homogeneous medium, both values approach 1.00, whereas tissue heterogeneity leads to

Table 4 Diagnostic performance of DWI parameters and MiAD for the differentiation of benign and metastatic RLNm

Parameters	AUC	Cutoff value	Youden index	Sensitivity	Specificity
ADC (μm²/ms)	0.671	0.686	0.301	0.822	0.478
DDC_{SEM} (μm²/ms)	0.814	0.647	0.536	0.667	0.870
α_{SEM}	0.846	0.746	0.601	0.644	0.957
D_{FROC} (μm²/ms)	0.793	0.636	0.476	0.911	0.565
β_{FROC}	0.810	0.748	0.562	0.867	0.696
μ_{FROC} (μm)	0.712	3.316	0.428	0.689	0.739
D_{CTRW} (μm²/ms)	0.800	0.703	0.536	0.667	0.870
β_{CTRW}	0.913	0.830	0.780	0.867	0.913
MiAD (mm)	0.727	9.3	0.366	0.844	0.522
Combined model	0.948	0.656	0.781	0.911	0.870

ADC Apparent diffusion coefficient, *AUC* Area under the curve, *CTRW* Continuous-time random walk model, *DWI* Diffusion-weighted imaging, *FROC* Fractional-order calculus model, *MiAD* Minimal axial diameter, *RLNs* Retropharyngeal lymph nodes, *SEM* Stretched-exponential model

Table 5 Logistic regression analyses of diffusion parameters for differentiating benign and metastatic RLNs

Variables	Univariable logistic regression	Multivariable logistic regression
	Odds ratio [95% CI] *p*-value	Odds ratio [95% CI] *p*-value
ADC (μm^2/ms)	0.991 [0.983–0.999] 0.036	NA NA
DDC_{SEM} (μm^2/ms)	0.983 [0.975–0.992] < 0.001	NA NA
α_{SEM}	1.029 [1.015–1.044] < 0.001	NA NA
D_{FROC} (μm^2/ms)	0.983 [0.974–0.992] < 0.001	NA NA
β_{FROC}	1.026 [1.013–1.039] < 0.001	NA NA
μ_{FROC} (μm)	1.003 [1.001–1.005] 0.006	NA NA
D_{CTRW} (μm^2/ms)	0.986 [0.978–0.993] < 0.001	NA NA
β_{CTRW}	1.050 [1.027–1.074] < 0.001	1.050 [1.027–1.074] < 0.001

ADC Apparent diffusion coefficient, *CTRW* Continuous-time random walk model, *CI* Confidence interval, *FROC* Fractional-order calculus model, *NA* Not applicable, *RLNs* Retropharyngeal lymph nodes, *SEM* Stretched-exponential model

their reduction [33–35]. A lower α_{CTRW} indicates that water molecules diffuse through a more temporally heterogeneous environment, whereas an increased β_{CTRW} suggests a more spatially homogeneous environment [33–38]. In this study, both benign and malignant RLNs exhibited reduced α_{CTRW} and β_{CTRW} values. However, a significant difference was observed in only β_{CTRW} values between the two groups. This discrepancy arises because different diffusion parameters reflect distinct aspects of tissue heterogeneity. Stimulation by factors such as inflammation and viral infections induced changes in the pathological microcirculation of RLNs, altering the diffusion of water molecules within them. These alterations were more pronounced in spatial rather than temporal diffusion heterogeneity. Similar dissociations between α_{CTRW} and β_{CTRW} have been reported in previous studies exploring lesions using the CTRW model. For instance, in a study comparing patients with Parkinson's disease and healthy controls [34], only β_{CTRW} exhibited a significant difference, while α_{CTRW} values remained comparable between the two groups. Conversely, a study differentiating prostate cancer from chronic prostatitis revealed significant differences in α_{CTRW} but not in β_{CTRW} values [35]. These findings suggest that α_{CTRW} and β_{CTRW} can characterize different types of changes in water molecule diffusion within lesions. Additionally, β_{CTRW} has demonstrated significant advantages in characterizing tissues with complex structures. For instance, in cervical cancer, β_{CTRW} exhibited superior diagnostic performance in differentiating squamous cell carcinoma from adenocarcinoma, with an AUC value of 0.836, compared to 0.664 for DDC_{SEM} and 0.642 for μ_{FROC} [37]. Furthermore, in a study predicting the Ki-67 proliferation index in cervical cancer, β_{CTRW} was identified as independent predictor, significantly enhancing the accuracy of the combined prediction model [38].

Morphological analysis of RLNs in this study showed that the MiAD was the only parameter significantly different between benign and metastatic lymph nodes, consistent with findings reported by Wang et al [20]. The diagnostic efficacy of the MiAD for distinguishing between benign and metastatic RLNs was 0.727, with a cutoff value of 9.3 mm, sensitivity of 84.4%, and specificity of 52.2%, respectively. Previous studies have also supported the utility of the MiAD in evaluating RLN metastasis [14, 15]. The current AJCC staging system lacks an optimal threshold for identifying metastatic RLNs [6]. Research has shown that a MiAD of 6.0 mm may be more appropriate than 5.0 mm [14, 15]. However, these size criteria are based on a normal population without infections or malignant lesions in the head or neck and, therefore, may not effectively differentiate benign reactive hyperplastic RLNs from metastatic lymph nodes [17–19].

Further analysis using receiver operating characteristic curves revealed that among the individual diffusion parameters, β_{CTRW} exhibited the highest diagnostic efficiency, with an AUC of 0.913, significantly outperforming ADC. This indicates that non-Gaussian parameters are more effective in reflecting tissue heterogeneity. Multivariate regression analysis confirmed β_{CTRW} as the optimal single diffusion indicator for differentiation. Combining β_{CTRW} with MiAD increased the AUC to 0.948, showing a significant improvement over all diffusion parameters except β_{CTRW} alone. These findings highlight the potential of advanced non-Gaussian diffusion models, when combined with morphological features, to provide a more comprehensive assessment of RLN heterogeneity and improve differentiation between benign and metastatic nodes, offering valuable clinical insights for treatment planning.

This study has some limitations. First, as a single-center, small cohort study, although this study initially validated the diagnostic value of diffusion parameters,

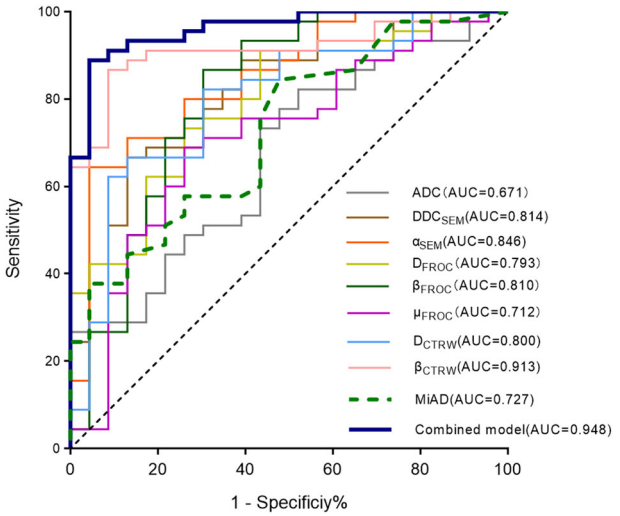

Fig. 5 Receiver operating characteristic curves of quantitative parameters for differentiating benign and metastatic RLNs. The combined model includes β_{CTRW} and the MiAD of lymph nodes. ADC, Apparent diffusion coefficient; CTRW, Continuous-time random walk; FROC, Fractional-order calculus; MiAD, Minimal axial diameter; RLNs, Retropharyngeal lymph nodes; SEM, Stretched-exponential model

further studies need to be validated by multicenter studies with large samples to confirm the efficacy of diffusion parameters in differentiating lymph nodes. Second, due to challenges in obtaining biopsies or resections of RLNs, histopathological data were unavailable. In this study, benign RLNs were identified based on MRI and endoscopic examinations in patients without nasopharyngeal or other head and neck cancers, with at least 1 year of clinical follow-up. To minimize false positives and negatives, both benign and metastatic lymph nodes were included based on a MiAD ≥ 6.0 mm. Third, diffusion parameters were measured using a two-dimensional ROI. A three-dimensional volume of interest (VOI) outlining the tissues may provide a more comprehensive assessment of heterogeneity. However, VOI delineation is labor-intensive and time-consuming, though artificial intelligence may offer a potential solution. Finally, although the current study preliminarily confirmed the value of non-Gaussian diffusion parameters in differentiating between benign and metastatic RLNs, the underlying biophysical mechanisms remain to be systematically elucidated. Therefore, future studies should focus on exploring the correlation mechanism between microenvironmental heterogeneity and diffusion patterns. This can be achieved using histopathology-radiomics registration technology to elucidate the relationship between tissue microstructure and diffusion heterogeneity coefficients. Additionally, it is necessary to quantify the impact weights of factors such as tumor cell proportion, microvessel density, and extracellular matrix on diffusion heterogeneity parameters. This will facilitate the transformation of imaging biomarkers into tools for individualized treatment decision-making.

In summary, non-Gaussian diffusion parameters derived from the CTRW, FROC, and SEM models play a significant role in distinguishing benign from metastatic RLNs, with β_{CTRW} being the most discriminative diffusion parameter. The combined application of β_{CTRW} and MiAD can further enhance diagnostic accuracy and holds promise as a noninvasive imaging biomarker for RLNs evaluation. This approach may facilitate the development of more precise clinical treatment strategies, reduce unnecessary or inappropriate radiotherapy, and provide essential imaging support for individualized treatment and prognostic assessment in NPC.

Abbreviations

ADC	Apparent diffusion coefficient
AUC	Area under the receiver operating characteristic curve
CTRW	Continuous time random walk model
DWI	Diffusion weighted imaging
EBV	Epstein-Barr virus
FROC	Fractional order calculus model
MiAD	Minimal axial diameter
MRI	Magnetic resonance imaging
NPC	Nasopharyngeal carcinoma
RLNs	Retropharyngeal lymph nodes
ROI	Region of interest
SEM	Stretched exponential model

Acknowledgements

We would like to thank Editage (www.editage.cn) for providing English language editing services. No large language models (LLMs), such as ChatGPT, Gemini, or Bard, or any other generative AI software, were used in the preparation of this manuscript.

Author contributions

JL, JZ, and YFQ devised the experiment. LH and FW designed the tables and figures. JL and YNS performed the data analysis. QY and MXL revised the manuscript. LJ wrote the original draft. The remaining authors were responsible for data collection. QY, JZ, and YFQ are co-corresponding authors. All authors have read and approved the final manuscript.

Funding

This study was supported by the Key Projects of Natural Science Research in Universities of Anhui Province (No. 2024AH050749) and Youth Science Fund Projects of Anhui Medical University (No. 2021xjk114).

Data availability

The data that support the findings of this study are available from YQ. Restrictions apply to the availability of these data, which were used under license for the current study, and therefore are not publicly available. Data are, however, available from the authors upon reasonable request and with permission from YQ.

Declarations

Ethics approval and consent to participate

This retrospective study was ethically approved by the Ethics Committee of Anhui Medical University. Ethics Number: 83244611, Effective Date: 4/18/2024.

Consent for publication

Written informed consent for publication of the images and data was obtained from the patient(s).

Competing interests

One of the authors (Mengxiao Liu) is an employee of Siemens Healthcare who mainly contributed to manuscript editing and did not participate in study design, data collection, analysis, or interpretation of this study. The other authors of this manuscript declare no relationships with any companies whose products or services may be related to the subject matter of the article.

Author details

[1]Department of Radiology, The First Affiliated Hospital of Anhui Medical University, Hefei, China. [2]Department of Medical Imaging, Anqing Medical Center of Anhui Medical University, Anqing, China. [3]Department of Laboratory Medicine, Anqing Medical Center of Anhui Medical University, Anqing, China. [4]MR Search & Marketing Department, Siemens Healthineers Co., Ltd., Shanghai, China. [5]Department of Radiology, The First Hospital of Lanzhou University, Lanzhou, China.

Received: 19 February 2025 Accepted: 16 April 2025
Published online: 13 May 2025

References

1. Chen YP, Chan ATC, Le QT et al (2019) Nasopharyngeal carcinoma. Lancet 394:64–80. https://doi.org/10.1016/S0140-6736(19)30956-0
2. Wang X, Hu C, Ying H et al (2015) Patterns of lymph node metastasis from nasopharyngeal carcinoma based on the 2013 updated consensus guidelines for neck node levels. Radiother Oncol 115:41–45. https://doi.org/10.1016/j.radonc.2015.02.017
3. Wang XS, Hu CS, Ying HM et al (2009) Patterns of retropharyngeal node metastasis in nasopharyngeal carcinoma. Int J Radiat Oncol Biol Phys 73:194–201. https://doi.org/10.1016/j.ijrobp.2008.03.067
4. Coskun HH, Ferlito A, Medina JE et al (2011) Retropharyngeal lymph node metastases in head and neck malignancies. Head Neck 33:1520–1529. https://doi.org/10.1002/hed.21526
5. Tang LL, Guo R, Zhou G et al (2014) Prognostic value and staging classification of retropharyngeal lymph node metastasis in nasopharyngeal carcinoma patients treated with intensity-modulated radiotherapy. PLoS One 9:e108375. https://doi.org/10.1371/journal.pone.0108375
6. Huang L, Zhang Y, Liu Y et al (2019) Prognostic value of retropharyngeal lymph node metastasis laterality in nasopharyngeal carcinoma and a proposed modification to the UICC/AJCC N staging system. Radiother Oncol 140:90–97. https://doi.org/10.1016/j.radonc.2019.04.024
7. Xu P, Min Y, Blanchard P et al (2017) Incidence of small lymph node metastases in patients with nasopharyngeal carcinoma: clinical implications for prognosis and treatment. Head Neck 39:305–310. https://doi.org/10.1002/hed.24586
8. Ghadjar P, Simcock M, Schreiber-Facklam H et al (2010) Incidence of small lymph node metastases with evidence of extracapsular extension: clinical implications in patients with head and neck squamous cell carcinoma. Int J Radiat Oncol Biol Phys 78:1366–1372. https://doi.org/10.1016/j.ijrobp.2009.09.043
9. Tang L, Mao Y, Liu L et al (2009) The volume to be irradiated during selective neck irradiation in nasopharyngeal carcinoma: analysis of the spread patterns in lymph nodes by magnetic resonance imaging. Cancer 115:680–688. https://doi.org/10.1002/cncr.24049
10. Kallehauge J, Nielsen T, Haack S et al (2013) Voxelwise comparison of perfusion parameters estimated using dynamic contrast enhanced (DCE) computed tomography and DCE-magnetic resonance imaging in locally advanced cervical cancer. Acta Oncol 52:1360–1368. https://doi.org/10.3109/0284186X.2013.813637
11. Liu Y, Zhang Y, Wang J et al (2023) Caudal distribution pattern of metastatic neck lymph nodes in nasopharyngeal carcinoma and prognostic significance of nodal spread distances. Radiother Oncol 179:109443. https://doi.org/10.1016/j.radonc.2022.109443
12. Lee AW, Ng WT, Pan JJ et al (2018) International guideline for the delineation of the clinical target volumes (CTV) for nasopharyngeal carcinoma. Radiother Oncol 126:25–36. https://doi.org/10.1016/j.radonc.2017.10.032
13. Shi Q, Shen C, Kong L et al (2014) Involvement of both cervical lymph nodes and retropharyngeal lymph nodes has prognostic value for N1 patients with nasopharyngeal carcinoma. Radiat Oncol 9:7. https://doi.org/10.1186/1748-717X-9-7
14. Zhu Y, Luo C, Zhou S et al (2024) Optimal size threshold for MRI-detected retropharyngeal lymph nodes to predict outcomes in nasopharyngeal carcinoma: a two-center study. AJR Am J Roentgenol 222:e2329984. https://doi.org/10.2214/AJR.23.29984
15. King AD, Woo JKS, Ai QY et al (2020) Early detection of cancer: evaluation of MR imaging grading systems in patients with suspected nasopharyngeal carcinoma. AJNR Am J Neuroradiol 41:515–521. https://doi.org/10.3174/ajnr.A6444
16. Yin H, Liu W, Xue Q et al (2024) The value of restriction spectrum imaging in predicting lymph node metastases in rectal cancer: a comparative study with diffusion-weighted imaging and diffusion kurtosis imaging. Insights Imaging 15:302. https://doi.org/10.1186/s13244-024-01852-z
17. Zhang GY, Liu LZ, Wei WH, Deng YM, Li YZ, Liu XW (2010) Radiologic criteria of retropharyngeal lymph node metastasis in nasopharyngeal carcinoma treated with radiation therapy. Radiology 255:605–612. https://doi.org/10.1148/radiol.10090289
18. Yu X, Yang F, Liu X et al (2022) Arterial spin labeling and diffusion-weighted imaging for identification of retropharyngeal lymph nodes in patients with nasopharyngeal carcinoma. Cancer Imaging 22:40. https://doi.org/10.1186/s40644-022-00480-4
19. Liang L, Luo X, Lian Z et al (2017) Lymph node metastasis in head and neck squamous carcinoma: efficacy of intravoxel incoherent motion magnetic resonance imaging for the differential diagnosis. Eur J Radiol 90:159–165. https://doi.org/10.1016/j.ejrad.2017.02.039
20. Wang P, Hu S, Wang X et al (2023) Synthetic MRI in differentiating benign from metastatic retropharyngeal lymph node: combination with diffusion-weighted imaging. Eur Radiol 33:152–161. https://doi.org/10.1007/s00330-022-09027-4
21. So TY, Ai QH, Lam WKJ et al (2020) Intravoxel incoherent motion diffusion-weighted imaging for discrimination of benign and malignant retropharyngeal nodes. Neuroradiology 62:1667–1676. https://doi.org/10.1007/s00234-020-02494-w
22. Kuai ZX, Sang XQ, Yao YF et al (2019) Evaluation of non-monoexponential diffusion models for hepatocellular carcinoma using b values up to 2000 s/mm^2: a short-term repeatability study. J Magn Reson Imaging 50:297–304. https://doi.org/10.1002/jmri.26563
23. Bedair R, Priest AN, Patterson AJ et al (2017) Assessment of early treatment response to neoadjuvant chemotherapy in breast cancer using non-mono-exponential diffusion models: a feasibility study comparing the baseline and mid-treatment MRI examinations. Eur Radiol 27:2726–2736. https://doi.org/10.1007/s00330-016-4630-x
24. Fujimoto K, Noda Y, Kawai N et al (2021) Comparison of mono-exponential, bi-exponential, and stretched exponential diffusion-weighted MR imaging models in differentiating hepatic hemangiomas from liver metastases. Eur J Radiol 141:109806. https://doi.org/10.1016/j.ejrad.2021.109806
25. Sui Y, Wang H, Liu G et al (2015) Differentiation of low- and high-grade pediatric brain tumors with high b-value diffusion-weighted MR imaging and a fractional order calculus model. Radiology 277:489–496. https://doi.org/10.1148/radiol.2015142156
26. Feng C, Wang Y, Dan G et al (2022) Evaluation of a fractional-order calculus diffusion model and bi-parametric VI-RADS for staging and grading bladder urothelial carcinoma. Eur Radiol 32:890–900. https://doi.org/10.1007/s00330-021-08203-2
27. Li Z, Dan G, Tammana V et al (2021) Predicting the aggressiveness of peripheral zone prostate cancer using a fractional order calculus diffusion model. Eur J Radiol 143:109913. https://doi.org/10.1016/j.ejrad.2021.109913
28. Wang C, Wang G, Zhang Y et al (2023) Differentiation of benign and malignant breast lesions using diffusion-weighted imaging with a fractional-order calculus model. Eur J Radiol 159:110646. https://doi.org/10.1016/j.ejrad.2022.110646

29. Wang F, Sun YN, Zhang BT et al (2024) Value of fractional-order calculus (FROC) model diffusion-weighted imaging combined with simultaneous multi-slice (SMS) acceleration technology for evaluating benign and malignant breast lesions. BMC Med Imaging 24:190. https://doi.org/10.1186/s12880-024-01368-4
30. Sheng R, Zhang Y, Sun W et al (2022) Staging chronic hepatitis B related liver fibrosis with a fractional order calculus diffusion model. Acad Radiol 29:951–963. https://doi.org/10.1016/j.acra.2021.07.005
31. Mao C, Hu L, Jiang W et al (2024) Discrimination between human epidermal growth factor receptor 2 (HER2)-low-expressing and HER2-overexpressing breast cancers: a comparative study of four MRI diffusion models. Eur Radiol 34:2546–2559. https://doi.org/10.1007/s00330-023-10198-x
32. Fan Z, Guo J, Zhang X et al (2024) Non-Gaussian diffusion metrics with whole-tumor histogram analysis for bladder cancer diagnosis: muscle invasion and histological grade. Insights Imaging 15:138. https://doi.org/10.1186/s13244-024-01701-z
33. Chang H, Wang D, Li Y et al (2023) Evaluation of breast cancer malignancy, prognostic factors and molecular subtypes using a continuous-time random-walk MR diffusion model. Eur J Radiol 166:111003. https://doi.org/10.1016/j.ejrad.2023.111003
34. Zhong Z, Merkitch D, Karaman MM et al (2019) High-spatial-resolution diffusion MRI in Parkinson disease: lateral asymmetry of the substantia nigra. Radiology 291:149–157. https://doi.org/10.1148/radiol.2019181042
35. Sheng Y, Chang H, Xue K et al (2024) Characterization of prostatic cancer lesion and Gleason grade using a continuous-time random-walk diffusion model at high b-values. Front Oncol 14:1389250. https://doi.org/10.3389/fonc.2024.1389250
36. Yang L, Hu H, Yang X et al (2024) Whole-tumor histogram analysis of multiple non-Gaussian diffusion models at high b values for assessing cervical cancer. Abdom Radiol (NY) 49:2513–2524. https://doi.org/10.1007/s00261-024-04486-3
37. Su Y, Zeng K, Yan Z et al (2024) Predicting the Ki-67 proliferation index in cervical cancer: a preliminary comparative study of four non-Gaussian diffusion-weighted imaging models combined with histogram analysis. Quant Imaging Med Surg 14:7484–7495. https://doi.org/10.21037/qims-24-576
38. Gao M, Li S, Yuan G et al (2024) Exploring the value of arterial spin labeling and six diffusion MRI models in differentiating solid benign and malignant renal tumors. Eur Radiol Exp 8:135. https://doi.org/10.1186/s41747-024-00537-y
39. Moffat BA, Chenevert TL, Lawrence TS et al (2005) Functional diffusion map: a noninvasive MRI biomarker for early stratification of clinical brain tumor response. Proc Natl Acad Sci U S A 102:5524–5529. https://doi.org/10.1073/pnas.0501532102
40. Habrich J, Boeke S, Nachbar M et al (2022) Repeatability of diffusion-weighted magnetic resonance imaging in head and neck cancer at a 1.5 T MR-Linac. Radiother Oncol 174:141–148. https://doi.org/10.1016/j.radonc.2022.07.020
41. Jović A, Fila J, Gršić K et al (2020) Diffusion-weighted MRI: impact of the size of the ROI in detecting metastases in subcentimeter lymph nodes in head and neck squamous cell carcinoma. Neuroradiology 62:987–994. https://doi.org/10.1007/s00234-020-02449-1
42. Han X, Suo S, Sun Y et al (2017) Apparent diffusion coefficient measurement in glioma: influence of region-of-interest determination methods on apparent diffusion coefficient values, interobserver variability, time efficiency, and diagnostic ability. J Magn Reson Imaging 45:722–730. https://doi.org/10.1002/jmri.25405
43. Song C, Cheng P, Cheng J et al (2020) Differential diagnosis of nasopharyngeal carcinoma and nasopharyngeal lymphoma based on DCE-MRI and RESOLVE-DWI. Eur Radiol 30:110–118. https://doi.org/10.1007/s00330-019-06343-0
44. Kerr JR (2019) Epstein-Barr virus (EBV) reactivation and therapeutic inhibitors. J Clin Pathol 72:651–658. https://doi.org/10.1136/jclinpath-2019-205822
45. Moss DJ, Burrows SR, Silins SL et al (2001) The immunology of Epstein-Barr virus infection. Philos Trans R Soc Lond B Biol Sci 356:475–488. https://doi.org/10.1098/rstb.2000.0784

Publisher's Note